Behaviour of interlocking mortarless hollow block walls under in-plane Loading

Nor Azizi Safiee[1], Noor Azline Mohd Nasira[1], Ashraf Fawzy Ashour[2] and Nabilah Abu Bakara[1]
[1] Department of Civil Engineering, Faculty of Engineering, University Putra Malaysia, Malaysia
[2] School of Engineering, University of Bradford, UK

Corresponding author: norazizi@upm.edu.my,
Tel: 603-89464403; Fax : 603-86567129

Abstract

Experimental study of five full scale masonry wall panels subjected to prescibed pre-compressive vertical loading and increasing in-plane lateral loading is discussed. All five walls were constructed using interlocking mortarless load bearing hollow concrete blocks. The behaviour of wall in term of deflections along the wall height, shear strength, mortarless joint behaviour and local and overall failures under increasing in-plane lateral loading and pre-compressive vertical loading are reported and analysed. Simple strut-and-tie models are also developed to estimate the ultimate in-plane lateral capacity of the panel walls tested. The results indicate that, as the pre-compressive load increases, the in-plane lateral load capacity of walls increases. All walls tested failed due to diagonal shear and/or moderate toe crushing depending on the level of the pre-compressive load. The proposed strut-and-tie models were able to give reasonable predictions of the walls tested.

Keywords: In-plane Loading, Shear Strength, Mortarless Masonry, Dry Joint, Putra Block, Hollow Block, Dry-Stacked

INTRODUCTION

Mortarless structural wall systems constructed using blocks with interlocking keys are an attractive alternative to conventional block walls. The main feature of the interlocking hollow block mortarless system is the elimination of mortar layers and the blocks are interconnected through interlocking keys (protrusions and grooves). The goal in interlocking system is to assure efficient construction forming with well-aligned masonry structures even without skilled masons. In this kind of construction dry joints will be formed between the block courses.

There have been several attempts to develop interlocking hollow blocks in different parts of the world. In Putra Block system, the blocks are stacked on one another and three-dimensional interlocking protrusions are provided in the blocks to integrate the blocks into walls (Thanoon et al. 2004). The structural behavior of this system has been assessed by performing experimental tests under axial and eccentric loads (Najm, 2001 and Fares, 2005). Based on the available experimental results, strength correlation between individual blocks, prisms, and basic wall panels of interlocking mortarless hollow block masonry has been developed (Jaafar et al. 2005). Further analytical and experimental studies have been conducted on the interlocking mortarless masonry system (Alwathaf et al. 2005, Alwathaf, 2006, Jaafar et al. 2006, Thanoon et al. 2008a, Thanoon et al. 2008b). Masonry walls are usually subjected to simultaneous gravity load and lateral loading resulting from wind and/or seismic excitation. However, limited research has been carried out on the structural behaviour of interlocking mortarless masonry walls under in-plane lateral loading (Alwathaf, 2006 and Alwathaf, 2005). As such, additional research in this field will improve the existing knowledge and understanding of its complex behaviour. This paper presents test results of full scale mortarless walls subjected to in-plane vertical and lateral loading. It also explores the possibility of using simple equilibrium models to estimate the ultimate capacity of the walls tested.

EXPERIMENTAL PROGRAM

Five wall panels were tested under constant vertical pre-compressive loads ranging between 1 and 4 N/mm^2 to consider the gravity load and load from the upper storeys. Lateral load was applied gradually until failure in order to evaluate the in-plane structural behaviour. The wall panels were constructed using Putra blocks and were assembled without mortar layers and without reinforcements.

A total of five unreinforced mortarless masonry walls were tested. Dimensions and pre-compressive loads for the five walls are summarized in Table 1.

Fabrication of Wall Panels

All the wall panels were built according to the geometry shown in Fig. 1. The wall panels were constructed by using Putra block through running bond pattern.

The Putra hollow blocks have three different configurations known as stretcher block, corner block and half block. Each block is incorporated with interlocking key at its top. The details of each block are given in Table 2. Table 2 shows the average values for the mechanical properties of individual block units based on 18 samples for each unit. The stretcher block commonly used as a main unit in the construction of the walls. The corner block unit is used to fit at the end of the walls. While the half block is used to complete the courses of the wall so that vertical joints will be staggered. Figure 2 shows the arrangement of each block to form a prism which utilizes the function of interlocking key in aligning the courses and lock them in their position.

Test Setup and Instrumentation

The wall panels were constructed in a steel frame equipped with vertical and horizontal hydraulic jacks. The vertical loading was distributed on the top of wall through a distribution I-shape steel beam having an overall depth of 305mm and flange width of 150mm. The horizontally mounted hydraulic jack was used to apply lateral load at the top of the wall. To avoid local failure of masonry unit at the point of application of lateral load, a 50 mm thick steel plate was used to transfer the load from the jack. The first course (lowest course) of the wall was horizontally restrained, in order to avoid any sliding effects of the wall panel during lateral loading. The

lateral displacements were measured by linear variables differential transducer (LVDT) at three different points: top, middle and base of the wall as shown in Figure 3. Another LVDT set were also placed on the wall surface to monitor any out of plane deformations at three different locations on wall: base, middle and top of walls. The strains in walls tested were measured by strain gauges at several location of wall surface. Figure 3 shows the experimental setup and locations of LVDTs and strain gauges.

In-plane vertical and lateral loading

The experimental testing was conducted in two main stages. Initially, a vertical compressive load was applied by means of the vertical hydraulic jack and increased until the desired stress for each wall was imposed on the wall. The hydraulic jack was then controlled at this achieved stresses until the end of the test. Three different pre-compressive stresses were applied to the walls, namely 1.0, 2.0 and 4.0 N/mm^2 as shown in Table 1. Then the lateral load was applied in a small force increment using the horizontal hydraulic jack until complete failure of the wall tested.

EXPERIMENTAL RESULTS and DISCUSSIONS

Test results including load-displacement, the interaction between compressive stress and shear strength of walls and failure modes are collected and presented below.

In-plane Lateral Displacement

Figure 4 shows the in-plane lateral load versus in-plane lateral displacement at the top of the five wall panels tested. For comparison purposes, lateral displacement of all walls are presented in the same diagram. However, the in-plane lateral displacements for every two replicates (W1(I) and W1(II); and W2(I) and W2(II)) are similar, indicating high quality control of the construction and testing of walls. Generally, the lateral-load and lateral-displacement diagrams are characterized by nonlinear behaviour, reflecting the interaction between the block units and the mortarless dry joints during loading.

The variation in displacement characteristic among walls tested depicted in Figure 4 is mainly attributed to the different amount of pre-compressive load applied to each of wall. It also

indicates that the mortarless masonry assemblages exhibit a nonlinear behaviour with varying stiffness upon the in-plane pre-compressive loading. The walls have dry joints in horizontal and vertical directions. Therefore, the zigzag behaviour of displacement observed in Figure 4 can be attributed to the successive close-up of the vertical dry joints.

Figure 4 shows that the main characteristics of the in-plane lateral displacements are significantly influenced by the value of pre-compressive stress applied to the wall. For the same applied lateral load, W1 series under the lowest pre-compressive loading exhibits the highest in-plane lateral displacement compared with W2 and W3 series under higher pre-compressive load. In fact, Putra block allowed approximately 2 mm displacement for tolerances before interlocking keys may break. This shows that the interlocking between the blocks played its role after a slip of about 2 mm. Figure 4 also indicates that walls exhibit higher stiffness for higher pre-compressive load. After applying more than approximately 50% of the maximum load of each wall, the in-plane lateral displacement rapidly increases. The pre-compressive load is also able to increase the lateral load carrying capacity of walls, caused by the higher friction forces that develop in the mortarless dry joints between block courses as discussed later.

In Plane Lateral Displacement Profiles along the Wall Height

This section discusses the in-plane lateral displacement profile over the wall height exhibited by all specimens under in-plane loading. The profile of lateral displacements over height is plotted for five selected lateral loads in Figures 5 to 7. At low load levels, the in-plane lateral displacements of the wall increased mostly in a linear manner as the height of wall increased. At moderate load levels, the wall displacement shows some concave curvature along the wall height. Towards the higher loads, the in-plane lateral displacement rapidly increased at the mid height of the wall compared with that at the top of the wall as shown in Figures 5 to 7 for most walls under different pre-compressive loads. This is mainly attributed to the nonlinear effect of the wall system caused by the close up of vertical joints under loading. However, for W3, with higher pre-compressive loading, the wall displacement shows convex curvature along the wall

height at all load levels. This is possibly attributed to the effect of the bending displacement over the wall height that could be increased at that pre-compressive load. The characteristics of lateral displacement of interlocking mortarless walls is complicated due to the effect of many factors such as shear deformation, bending deformation and the relative movements along the dry jointsand local dry joint failure.

Failure Modes

Failure was controlled by diagonal shear cracks and/or moderate toe crushing. For low pre-compressive vertical load level, the wall failure was dominated by diagonal shear cracks. The shear failure was characterized by the development of bed joints sliding and vertical joints opening, contributing to the development of stepped diagonal cracks without visible cracking in the block units as shown in Fig. 8 for W1 and W2. These cracks were initiated by tension splitting of masonry in the compression strut formed in the wall as also observed by Voon and Ingham, (2007). This type of failure mode was possible due to the existence of axial pre-compressive loads. This failure mode is similar to that exhibited by the dry joint system tested by Lourenco (2005).

For higher pre-compressive vertical load level, the wall (W3) was failed due to toe crushing as shown in Figure 8 owing to the high pre-compressive vertical load applied to the wall that delayed any possible sliding along the bed joints but caused crushing at toe. Cracking through the block unit was also noticeable. Toe or corner crushing failure of the wall occurred due to the principal compressive stresses reaching the diagonal compressive strength of block units.

Pre-compressive stress and shear strength relationship

The main outcome from the in-plane wall testing investigation is the development of a relationship between average pre-compressive stress and shear stress at failure, where the average shear stress represents the measured failure lateral load divided by the horizontal cross section of the walls tested. The pre-compressive vertical loads and maximum lateral loads at

failure for all walls tested are summarized in Table 3. As mentioned previously, the maximum lateral load increases with the increase of the pre-compressive load which best presented using Mohr-Coulomb formulation where the criterion indicates that the shear strength increases as the axial compressive stress increases. In Mohr-Coulomb formulation, the related parameters represent this behaviour will be the shear stress at failure, τ, friction coefficient in joint interface, μ and the cohesion, c. Figure 9 shows the relationship between the pre-compressive vertical stress and lateral shear stress obtained from the current experimental investigation, Lourenco (2005) and Velmelfoort (1993), with linear regression lines to fit test results obtained from each investigation. Figure 9 also indicates that the mortarless wall system is able to resist the shear stress induced by in-plane lateral load with the assistance of the pre-compressive vertical loads without mortar layers. In Figure 9, the normal (σ) and shear (τ) stresses were calculated by dividing the pre-compressive and lateral loads by normal area of bedded face-shell which is calculated as the wall length (1.5m) times the wall effective thickness. The effective thickness was the net thickness of the face shells only (hollow block). The linear regression computed for the five walls showed relatively a good approximation to the experimental data with a correlation coefficient $R^2 = 0.826$. The linear regression relationship between shear stress and normal stress at failure is:

$$\tau = 0.2267\sigma + 0.31 \quad (1)$$

The approximation of linear regression resulted in high cohesion which gives the strength value at zero pre-compressive stress. Furthermore as a comparison, results from different systems of dry joints without interlocking masonry (Lourenco, 2005) is also plotted in Figure 9 . The results from dry joint without interlocking show small value of cohesive parameter compared to other systems.

The block bed geometric imperfection occurred during the casting process of wall blocks induces irregular interface in addition to their surface roughness, which affect the shear strength of dry joints. The friction resistance of bed joint area was not fully utilized, which causes stress concentration at localized areas as observed in Figure 10. Therefore, the unevenness of bed joint significantly decreases the shear strength of the system.

The mortarless dry joint has zero cohesion between the block courses (Alwathaf, 2006 and Lourenco, 2004). This means the relation should pass through the origin point. Furthermore, for higher pre-compressive stress $\sigma_n > 2.0$ N/mm^2, the relationship between shear stress and pre-compressive stress become nonlinear due to the material failure of the wall system as also observed by Guo (1991). Therefore, the previous result is better to be presented by power regression line which gives a correlation coefficient $R^2 = 0.90$. The relationship between shear strength and pre-compressive stress obtained from this analyses is $\tau_v = 0.4847\sigma_n^{0.6946}$ as shown in Fig. 11.

To compare friction coefficient of the system with other systems, the pre-compressive stress of 1.0 and 2.0 N/mm^2 are used only in linear relation. This gives a friction coefficient around 0.42. This is low compared to bonded (mortared) masonry which provides 0.6 for friction coefficient (BSI, 1992) but it is still higher than some bonded walls, for example bonded walls tested by Velmelfoorth (1993) exhibited a friction coefficient of 0.33. As a comparison with another mortarless masonry system, the obtained friction coefficient value is higher (Lourenco, 2005) as shown in Fig. 9. It is to be noted that the investigations by Lourenco (2005) and Velmelfoorth (1993) were conducted on dry masonry walls without interlocking system and conventional mortar walls, respectively. In addition to this, the effectiveness of mortarless system could be improved by using higher pre-compressive load for both systems; with interlocking and without interlocking masonry unit. It is important to indicate that the imperfection of the block bed is

highly affecting the shear strength of the system as it causes a reduction in the contacted areas (Alwathaf, 2005).

Strut-and-tie model for in-plane loaded masonry walls

There are various failure modes observed in masonry walls under in-plane vertical and horizontal loads. The diogonal shear cracking failure mode observed in W1 and W2 series, combined with toe crushing observed in W3 would be best represented by strut and tie models. The strut-and-tie model provides a rational approach by representing a complex structure member with an appropriate simplified truss model. It has not been widely applied to masonry structures in comparisons with reinforced concrete structures. In this section, the strut-and-tie approach will be utilized for the prediction of wall load capacity. The effectiveness of the proposed strut-and-tie models will be exaimned by comparing their predictions with experimental results from this study.

The strut and tie model is principally based on the failure mechanism observed in the physical wall testing. The equilibrium conditions at nodes are then employed in calculating forces in struts and ties. Figure 12 shows an idealized strut-and-tie model for walls failed in diagonal shear, similar to W1 and W2. This model is a combination between parallel and fan struts, similar to the model proposed by Roca (2006).

Considering equilibrium of forces in parallel struts and in-plane loads as shown in Figure 12(b), the following relations between forces are driven:

$$H_1 = S_1 \sin \beta_1 \tag{2}$$

$$V_1 = S_1 \cos \beta_1 \tag{3}$$

where S_1 is the force in parallel struts, V_1 is the in-plane vertical force acting on the parallel strut zone, H_1 is the in-plane lateral load required for horizontal force equilibrium and β_1 is the parallel strut angle with the vertical axis as shown in Fig. 12.

The in-plane vertical force V_1 acting on the parallel strut zone can be written in the following form:

$$V_1 = \frac{V(b-b_f)}{b} \tag{4}$$

where V is the total in-plane vertical load, b and b_f are the wall length and fan length as shown in Figure 12.

Combining Eqs. (2), (3) and (4), the in-plane horizontal force H_1 may be written as below:

$$H_1 = \frac{V(b-b_f)}{b} tan\beta_1 \tag{5}$$

For the case of fan strut, an average angle β_2 of fan strut was chosen to simplify the complexity of fan strut capacity evaluation. Considering the free body diagram for fan strut shown in Figure 1(c) and by following similar steps to the parallel strut capacity calculation, the horizontal component H_2 of the fan strut capacity is obtained below:

$$H_2 = V_2 \tan\beta_2 \tag{6}$$

where S_2 is the fan strut capacity, V_2 is the vertical component of the fan strut capacity, β_2 is the average fan strut angle relative to the vertical axis. As $V_2 = \frac{Vb_f}{b}$, H_2 may be written in the following form:

$$H_2 = \frac{Vb_f}{b} \tan\beta_2 \tag{7}$$

Therefore, total horizontal in-plane horizontal load capacity of wall is:

$$H = H_1 + H_2$$

$$= \frac{V}{b}\left(b \tan\beta_1 + b_f(\tan\beta_2 - \tan\beta_1)\right) \tag{8}$$

At ultimate condition and for mortarless/dry joint case, β_1, β_2 and the angle of internal friction ϕ of masonry are related to each other with the following relation (Roca 2006):

$$\beta_2 = \frac{\beta_1}{2} = \frac{\phi}{2} \tag{9}$$

The top length b_f of the fan strut is calculated from:

$$b_f = a + h tan\beta_1 \tag{10}$$

where h is the wall height and a is the node dimension at the toe where crushing occurred. a can be calculated from:

$$a = \frac{V_2}{tf_c} = \frac{Vb_f}{btf_c} = \mu b_f \tag{11}$$

where f_c is the compression strength of masonry wall, t is the masonry wall thickness and $\mu = V/(btf_c)$. Using Eqs. 9 and 11, the value of b_f may be written in the following form:

$$b_f = h \tan \emptyset \left(\frac{1}{1-\mu}\right) \tag{12}$$

Therefore, substituting the value of b_f in Eq. 8, the total horizontal in-plane horizontal load capacity can be calculated for this strut-and-tie model.

Table 4 presents the prediction of the in-plane lateral load capacity obtained from Eq. 8 for W1 and W2. The ratios for the prediction to experimental in-plane lateral load capacities for W1 and W2 are 0.91 and 0.90, respectively. These results indicate that the proposed strut and tie model is able to predict the in-plane lateral load capacity with reasonable accuracy.

An alternative strut-and-tie model shown in Figure 13 consists of a main diagonal strut with nodes at the top and bottom of the wall where the in-plane lateral loads applied. From the wall geometry, the diagonal strut inclination θ with the horizontal axis can be calculated as:

$$\tan \theta = \frac{h-c}{b-a} \tag{13}$$

where h and b are the wall vertical and horizontal dimensions, c and a are the node dimensions as shown in Figure 13. The value of c may be considered the same as the end plate through

which the in-plane lateral load applied. The angle θ of compressive strut for the walls tested in this investigation is $\theta = 47^0$.

Due to masonry crushing at the toe region, the compressive stresses σ_s at the wall toe has achieved the effective masonry compressive strength, νf_c as below:

$$\sigma_x = \nu f_c \tag{14}$$

where f_c is the masonry compressive strength and ν is the effectiveness factor of compressive strength of masonry. Several researchers (Patrick, 2015; Laurenco et al, 2006; Foraboschi and Vanin, 2010) have developed strut and tie models for designing masonry walls. The effectiveness factor ν proposed by Lourenco et al (2006) will be used in the current investigation to modify the brickwork compressive strength as below:

$$\upsilon = 0.8\beta_s\beta_\alpha \tag{15}$$

where βs is the strut efficiency factor, taken as 0.75 and β_α is the strut inclination factor, taken as 2/3 for inclination angle ≥ 37.5^0 (Lourenco et al (2006)).

Therefore, the in-plane lateral load H can be calculated by multiplied σ_x and the bearing area as below:

$$H = \sigma_x \; c\, t = \nu f_c \; c\, t \tag{16}$$

where t is the masonry wall thickness. The prediction of Eq. (16) for the in-plane lateral load capacity of W3 is 120.0 kN using the value of ν obtained from Eq. (15), well agree with the experimental value of 136.8 kN.

CONCLUSIONS

The behaviour of mortarless interlocking load bearing hollow block wall panels under combined in-plane vertical and lateral loading was investigated. The mortarless walls subjected to in-plane loads exhibited a nonlinear lateral displacement with increasing stiffness upon increasing pre-

compressive vertical load applied on the wall. This investigation revealed that, pre-compressive load able to increase the lateral load carrying capacity of walls which caused by the higher friction forces that develop in the mortarless dry joints. As the results, when the pre-compressive load increases, shear resistance also increases. It was concluded that pre-compressive load become a significant factor on the in-plane shear capacity of mortarless walls.

The failure modes of mortarless wall under in-plane load were controlled by diagonal shear failure and/or moderate toe crushing depending on the level of pre-compressive load. Shear failure characterized by development of sliding along bed joints and opening of vertical joints contributed to a stepped diagonal crack without visible cracking in the blocks for low and moderate pre-compressive loads. The power relation is the best fit relation that takes into consideration the zero cohesion of dry joints as well as the material failure at the higher pre-compressive load for the interlocking mortarless wall system. The comparison with other bonded and unbounded masonry system show an acceptable behaviour of the studied masonry system.

The developed strut-and-tie model is a practical tool for predicting the in-plane lateral load capacity of masonry walls.

REFERENCES

Alwathaf A. H., Thanoon W. A. M., Noorzaei J., Jaafar M. S. and Abdulkadir M. R. 2005. Shear Characteristic of Interlocking Mortarless Block Masonry Joints. *Masonry International*, Journal of the British Masonry Society, Vol.18, No.3, pp.139-146.

Alwathaf, A.H. 2006. Development of finite element code for non-linear analysis of interlocking mortarless masonry system, PhD thesis, Civil Engineering Department, University Putra Malaysia

British Standard Institution (1992). Code of Practice for Use of Masonry Part 1: Structural Use of Un-reinforced Masonry. BS 5628: Part 1, BSI, London

Fares A. Shehab. 2005. Structural behaviour of Interlocking hollow block panel with stiffener subjected to axial and eccentric load, Master thesis, Universiti Putra Malaysia

Guo, P. (1991). *Investigation and Modelling of the Mechanical Properties of Masonry*, Ph. D. Thesis, McMaster University. Hamilton, Ontario, Canada.

Jaafar, M. S., Thanoon, W.A., Najm, A.M.S, Kadir, M.R.A, Abang A.A.A, 2006, Strength correlation between individual block, prism and basic wall panel for load bearing interlocking mortarless hollow block masonry, Construction and Building Material, 20: 492-498

Jaafar, M. S., Alwathaf, A. H., Thanoon, W. A., Noorzaei, J. and AbdulKadir, M. R. (2006), Behaviour of Interlocking Mortarless Block Masonry. *Proceedings of ICE, Construction Materials*, Vol.159, No.3, pp.111-117.

Lourenco, P. B., Ramos, L. F., 2004, Characterization of Cyclic Behavior of Dry Masonry Joints, Journal of Structural Engineering, Vol. 130, 779-786

Lourenco, P.B., Oliveira, D. V., Roca, P., Orduna, A. 2005, Dry joint stone masonry walls subjected to in-plane combined loading, Journal of Structural Engineering, 131 (11): 1665-1673

Najm, A.M.S., 2001. Structural behaviour of load-bearing interlocking hollow block masonry, Master thesis, Universiti Putra Malaysia

Thanoon, W.A., Jaafar, M. S., Kadir, M.R.A, Abang, A.A.A., Trikha D.N., Amad M.S.N, 2004, Development of an innovative interlocking load bearing hollow block system in Malaysia, Construction and Building Materials, Vol. 18 (6): 445-454

Thanoon, W. A., Alwathaf, A. H., Noorzaei, J., Jaafar, M. S. and AbdulKadir, M. R. (2008), Finite Element Analysis of Interlocking Mortarless Hollow Block Masonry Prism. *Computer & Structures*, Vol.86, No.6 (March), pp.520-528.

Thanoon, W. A., Alwathaf, A. H., Noorzaei, J., Jaafar, M. S. and AbdulKadir, M. R. (2008), Non-Linear Finite Element Analysis of Grouted and Un-Grouted Hollow Interlocking Mortarless Block Masonry System. *Engineering Structures*, Vol.30, pp.1560-1572.

Velmelfoort ATh and Raijmakers TMJ. (1993). Deformation controlled tests in masonry shear walls, Part 2. Report TUE/BKO/93.08, Eindhoven University of Technology, Eindhoven.

Voon, K.C and Ingham, J.M. (2007). Design Expression for the In-Plane Shear Strength of Reinforced Concrete Masonry. Journal of Structural Engineering, Vol. 133, pp. 706-713

Table 1 Detail of Test Wall Panels

Specimen	Panel Size (H x L)	Pre-compressive Stress (N/mm^2)	Pre-compressive Load (kN)
W1 (I)	1600 x 1500	1.0	120
W1 (II)	1600 x 1500	1.0	120
W2 (I)	1600 x 1500	2.0	240
W2 (II)	1600 x 1500	2.0	240
W3 (I)	1600 x 1500	4.0	480

Table 2 Details of Putra hollow block

Block	Dimensions (L x H x t) mm	Comp. strength f'_c (N/mm^2)	Tensile strength, f'_t (N/mm^2)
Stretcher interlocking key 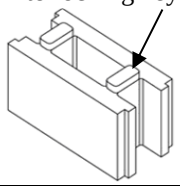	300 x 200 x 150	22.85 (COV: 16.5)	2.06 (COV: 5.31)
Half 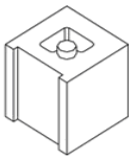	150 x 200 x 150	22.02 (COV: 16.4)	2.16 (COV: 9.72)
Corner 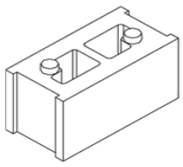	300 x 200 x 150	23.67 (COV: 13.7)	2.79 (COV: 15.36)

Table 3 Vertical and maximum lateral loads measured

Specimen	Normal force (kN)	Pre-compressive stress (N/mm^2)	Max lateral Load (kN)	Max shear stress (N/mm^2)
W1 (I)	120	1.0	58.30	0.486
W1 (II)	120	1.0	52.05	0.434
W2 (I)	240	2.0	93.72	0.781
W2 (II)	240	2.0	117.20	0.977
W3 (I)	480	4.0	136.8	1.14

Table 4 Prediction of strut-and-tie model shown in Fig. 12 for W1 and W2

Wall	V(kN)	b(mm)	h(mm)	t(mm)	f_c (N/mm^2)	β_1	H_{exp} (kN)	H_{pre} (kN)	H_{pre}/H_{exp}
W1	120	1500	1600	150	10.0	37	55.2	50.01	0.91
W2	240	1500	1600	150	10.0	43	105.5	95.23	0.90

List of Figure Captions

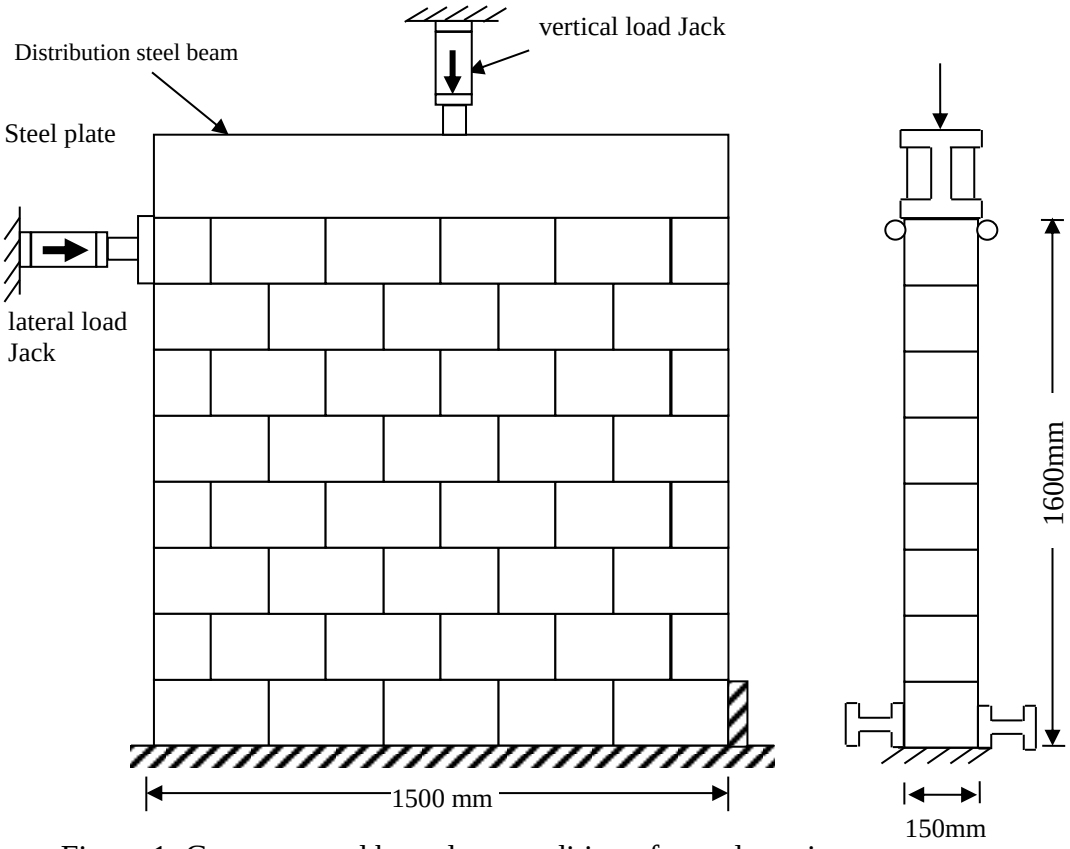

Figure 1: Geometry and boundary condition of tested specimen

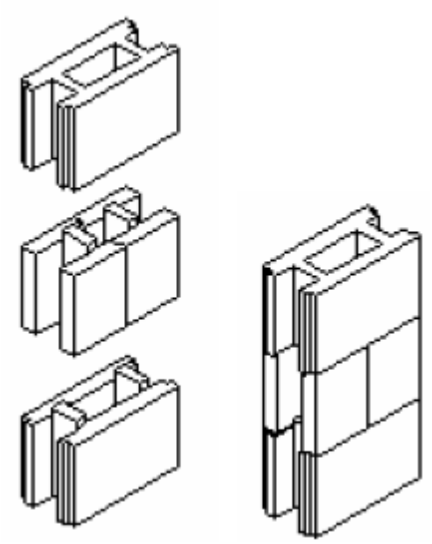

Figure 2 Assembly of interlocking blocks to form a vertical prism

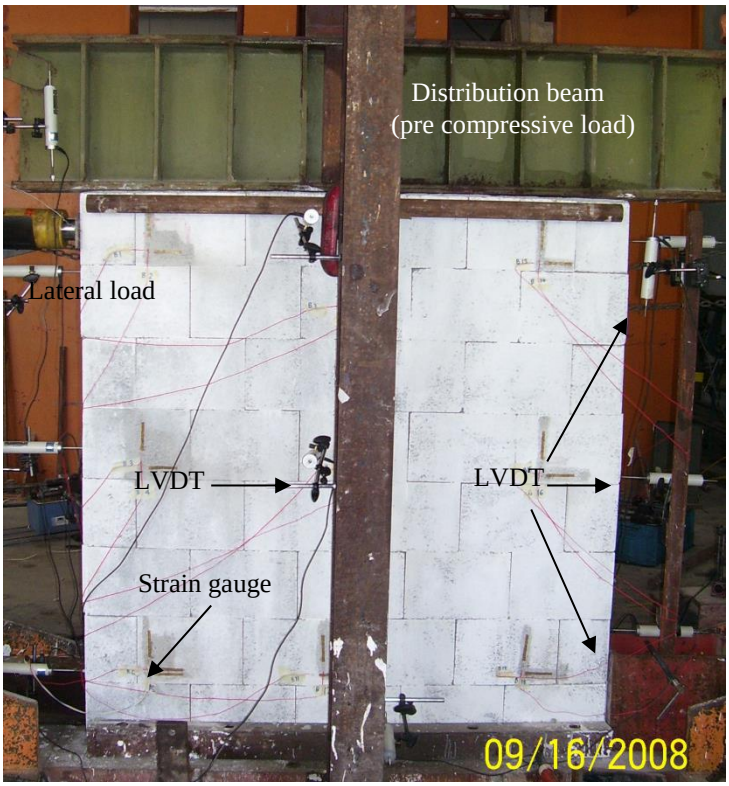

Figure 3: Test Setup and Instrumentation

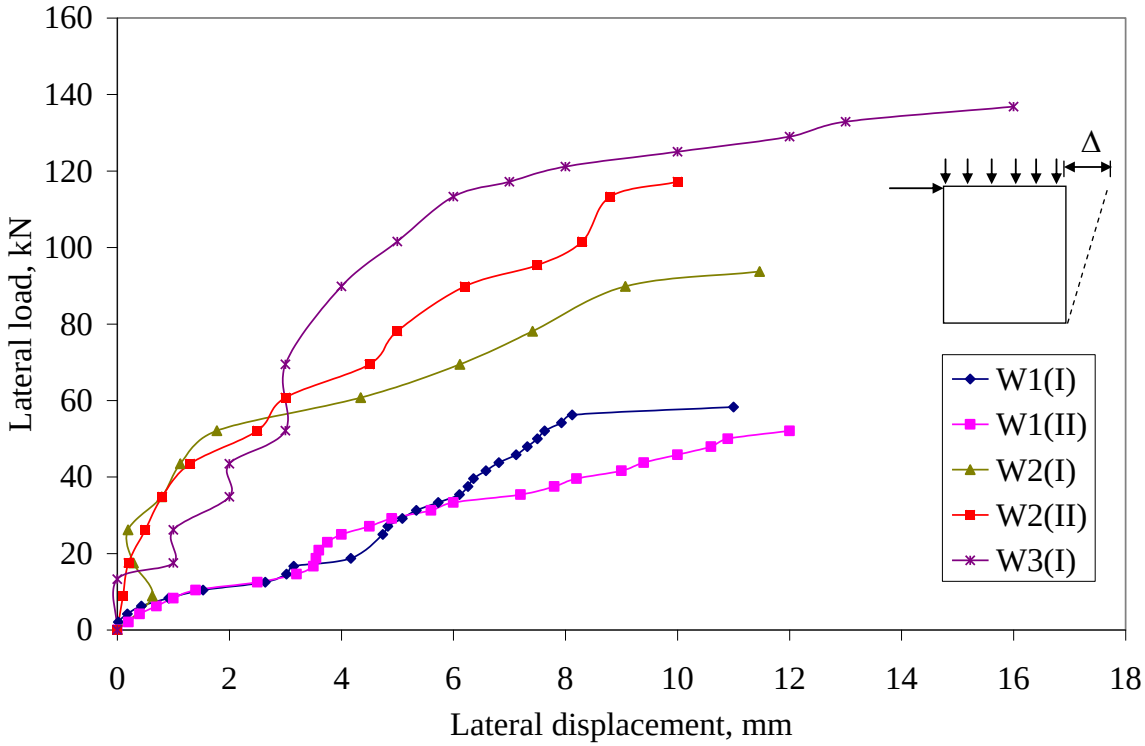

Figure 4: In-plane Lateral load vs Lateral Displacement

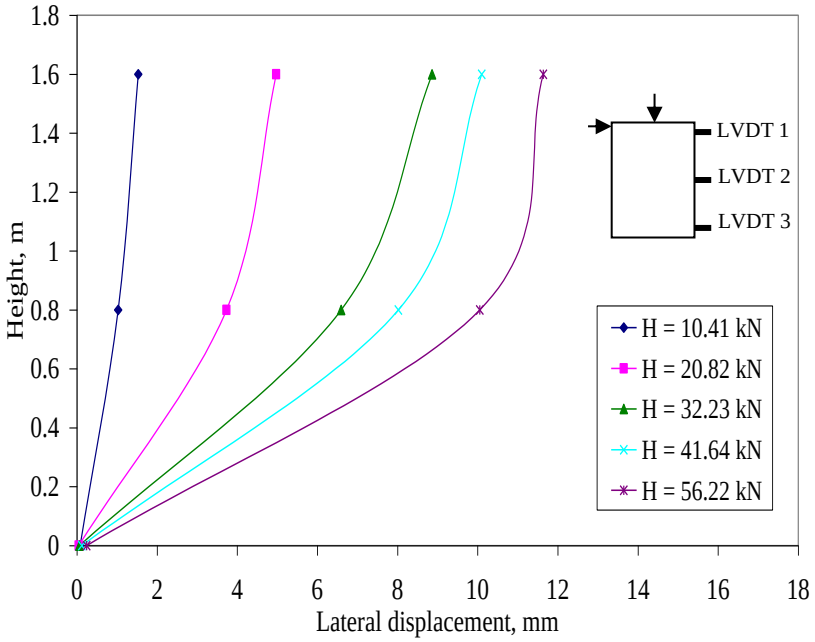

(i) W1 (I)

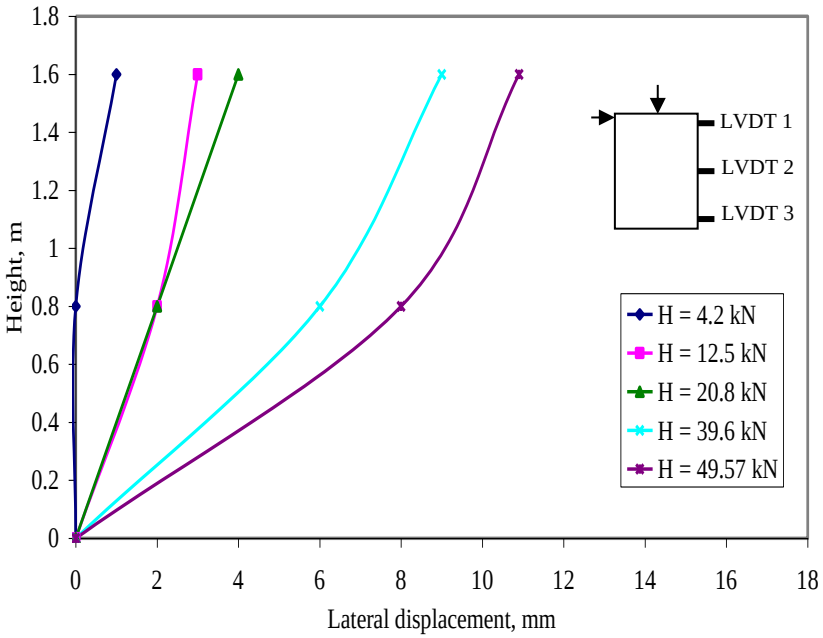

(ii) W1 (II)

Figure 5: Lateral displacement profile of W1 series

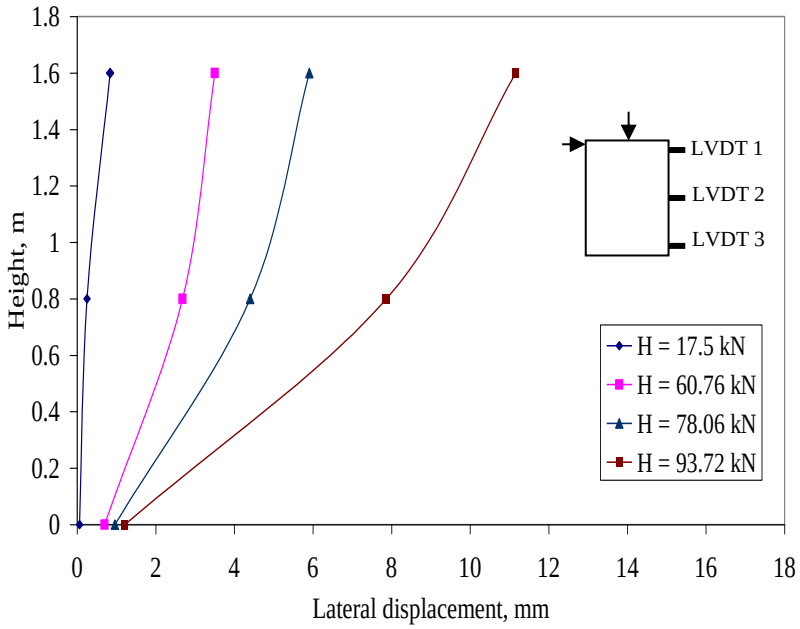

(i) W2 (I)

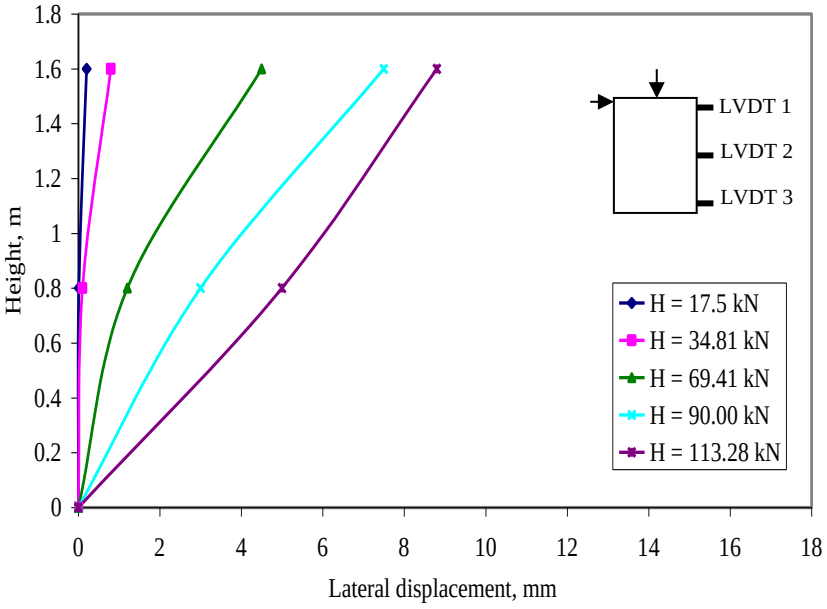

(ii) W2 (II)

Figure 6 : Lateral displacement profile of W2 series

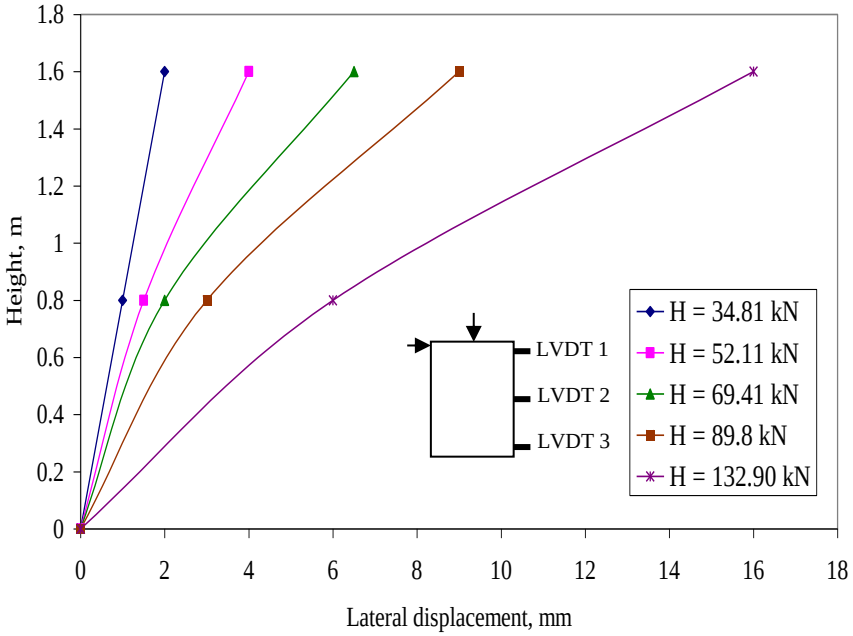

Figure 7 : Lateral displacement profile of W3 series

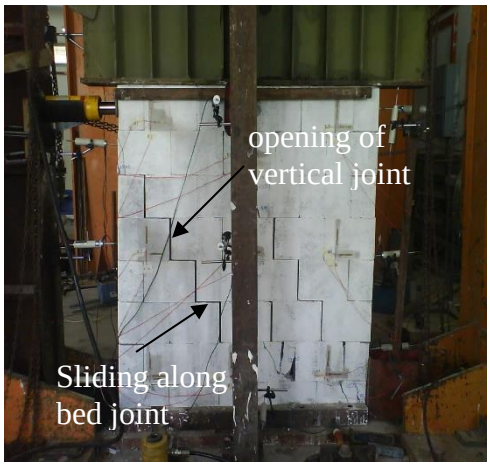

(i) W1

(ii) W2

(iii) W3

Figure 8: Failure Pattern of the Wall Panels

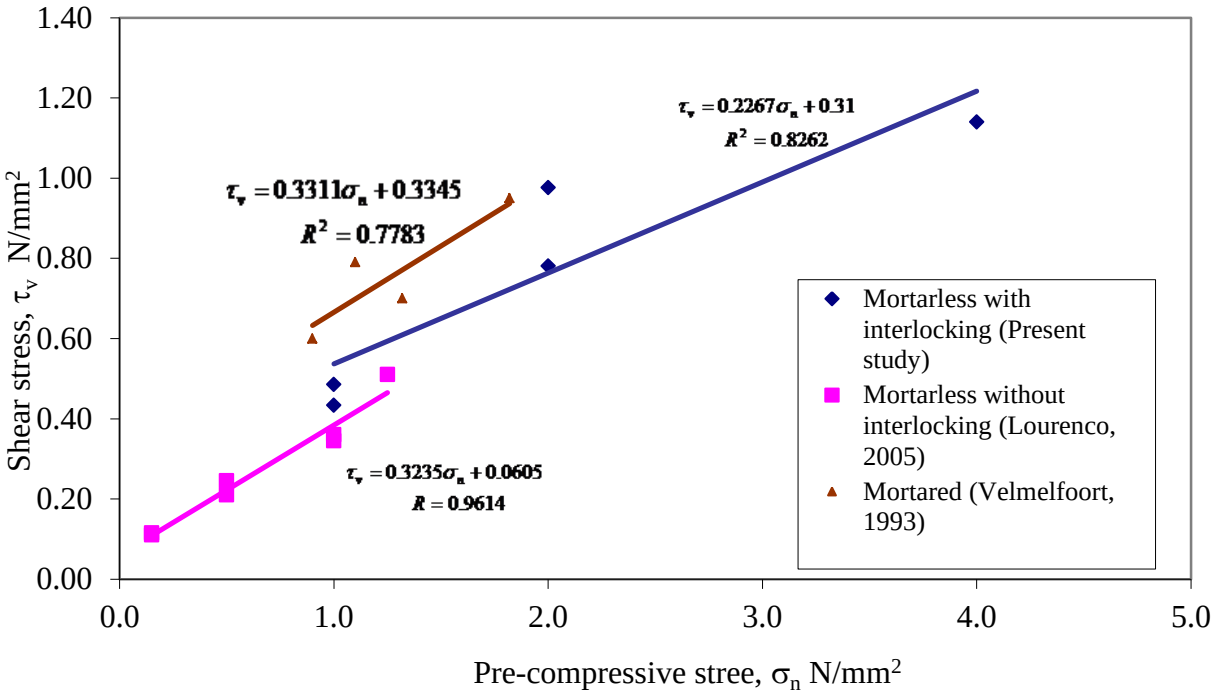

Figure 9: Relationship between Pre-compressive Normal Stress and Shear Stress

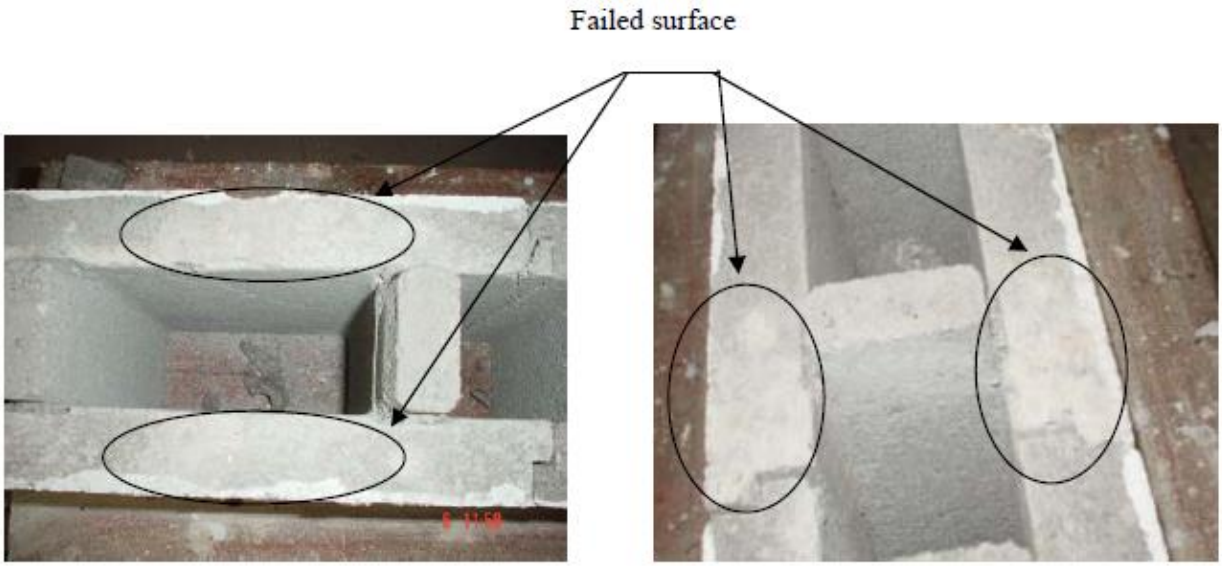

Figure 10: Surface roughness of face shell bed joint of block unit.

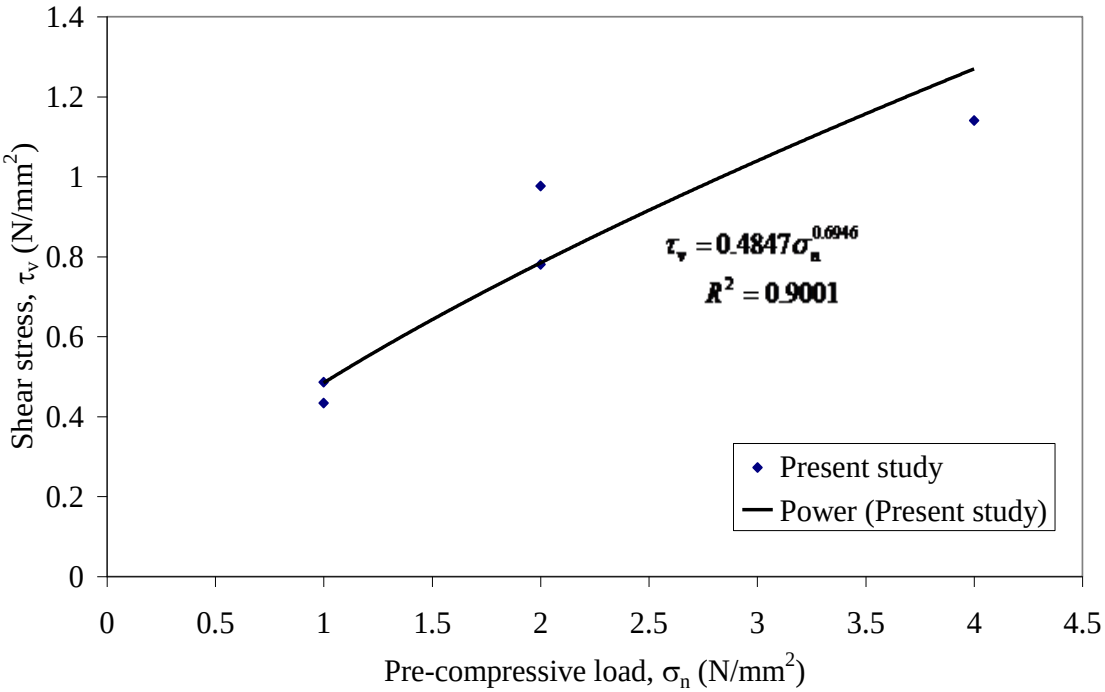

Figure 11: Nonlinear relationship between Pre-compressive Normal Stress and Shear Stress.

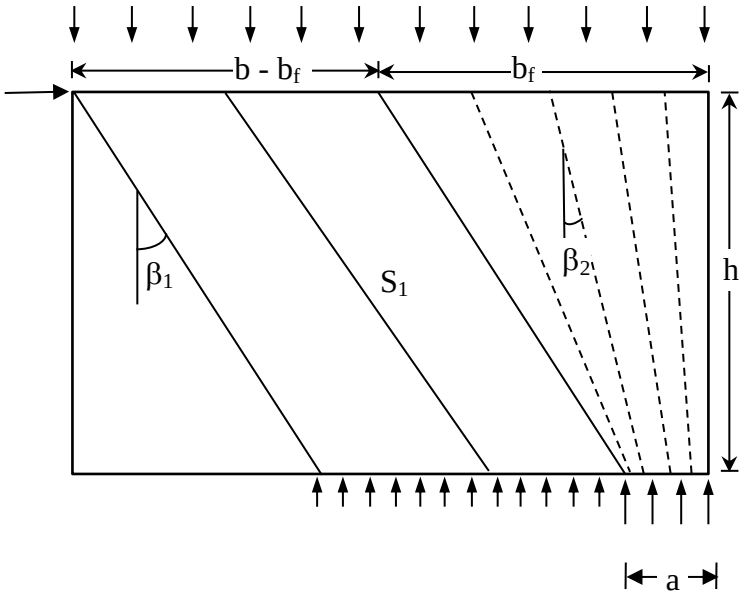

(a) Proposed parallel smeared and fan struts

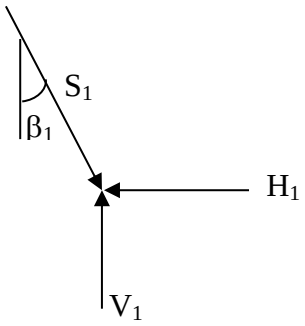

(b) Equilibrium of forces at the wall base for parallel struts

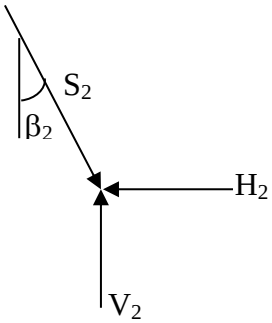

(c) Equilibrium of forces at node of base of wall for fan strut, S_2

Figure 12 proposed strut-and-tie model for W1 and W2 walls.

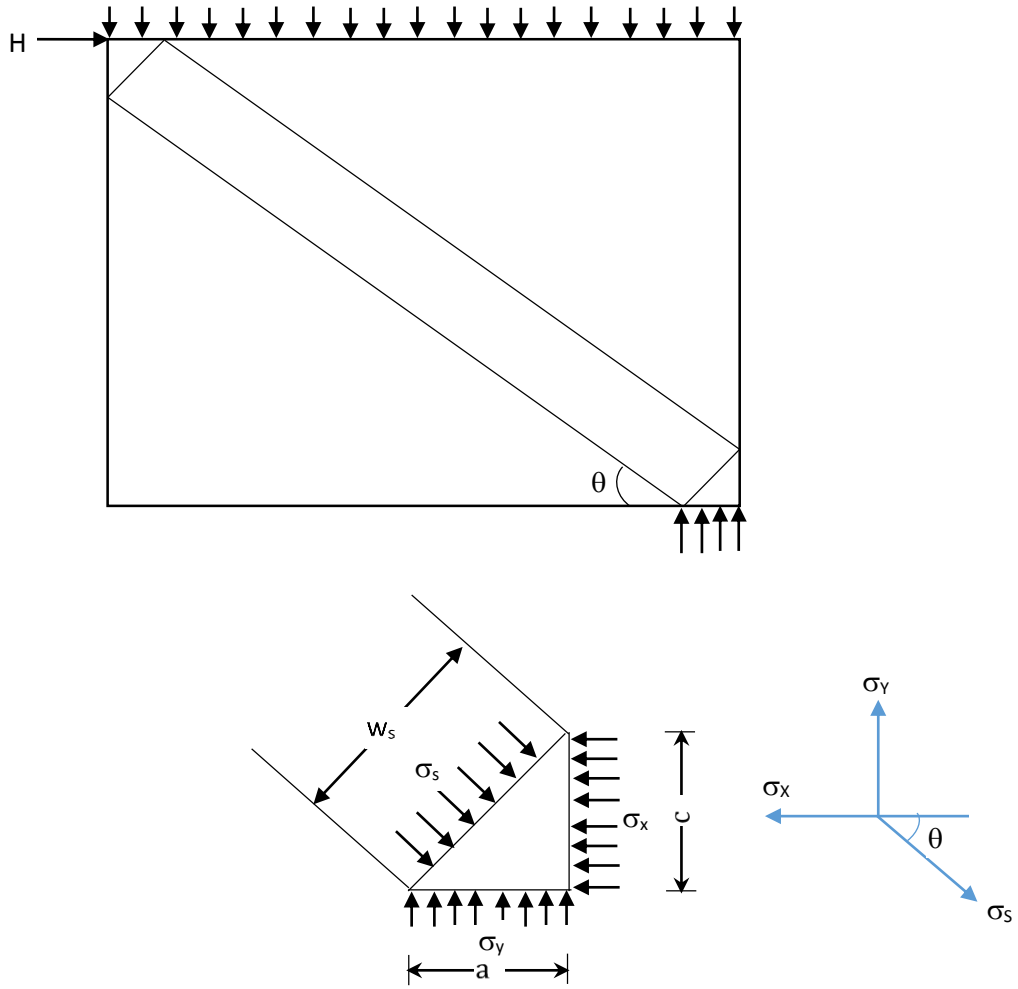

Figure 13 proposed strut-and-tie model for W3 wall.